Appl. Phys. B 85, 295–300 (2006)
DOI: 10.1007/s00340-006-2355-2

Applied Physics B
Lasers and Optics

A.A. KOSTEREV✉
T.S. MOSELY
F.K. TITTEL

Impact of humidity on quartz-enhanced photoacoustic spectroscopy based detection of HCN

Department of Electrical and Computer Engineering, Rice University, 6100 Main Street, Houston, TX 77005, USA

Received: 9 May 2006/Revised version: 5 June 2006
Published online: 14 July 2006 • © Springer-Verlag 2006

ABSTRACT The architecture and operation of a trace hydrogen cyanide (HCN) gas sensor based on quartz-enhanced photoacoustic spectroscopy and using a $\lambda = 1.53\,\mu$m telecommunication diode laser are described. The influence of humidity content in the analyzed gas on the sensor performance is investigated. A kinetic model describing the vibrational to translational (V–T) energy transfer following the laser excitation of a HCN molecule is developed. Based on this model and the experimental data, the V–T relaxation time of HCN was found to be $(1.91 \pm 0.07)10^{-3}$ s Torr in collisions with N_2 molecules and $(2.1 \pm 0.2)10^{-6}$ s Torr in collisions with H_2O molecules. The noise-equivalent concentration of HCN in air at normal indoor conditions was determined to be at the 155-ppbv level with a 1-s sensor time constant.

PACS 82.80.Kq; 42.62.Fi

1 Introduction

Hydrogen cyanide (HCN) is a highly toxic chemical species. It is used in a variety of industrial syntheses including the production of adiponitrile (for nylon), methyl methacrylate, pharmaceuticals, and other specialty chemicals. Manufacturing activities releasing hydrogen cyanide include electroplating, metal mining, metallurgy, and metal-cleaning processes. Besides, HCN is considered as a warfare chemical agent. The National Institute for Occupational Safety and Health (NIOSH) has established a recommended exposure limit (REL) for hydrogen cyanide of 4.7 ppmv (5 mg/m^3) as a short-term exposure limit (STEL) [1]. Therefore, the development of a HCN sensor capable of detecting sub-ppmv concentration levels and operating in an industrial environment is an important step toward ensuring industrial safety. Hydrogen cyanide is also formed during the incomplete combustion of nitrogen-containing polymers, such as certain plastics, polyurethanes, wool, and paper. Therefore, HCN detection is important in early fire detection on board of an aircraft or spacecraft.

In this work we report the design and performance evaluation of a HCN sensor based on the quartz-enhanced photoacoustic spectroscopy (QEPAS) technology [2]. The QEPAS approach has been previously used for the quantification of trace concentrations of a number of small molecules, as reported in [2]. The sensitivity to a chemical species when normalized to the absorption line strength and the excitation laser power is primarily determined by the rate of vibrational to translational (V–T) energy transfer, reaching its maximum when this rate is higher than the laser modulation frequency. This rate may depend on the major composition of the gas carrying the target trace component. In particular, the presence of H_2O in air can affect V–T energy transfer. Hence, the impact of humidity on the sensor performance must be characterized in order to use such a sensor in a real-world environment. In this work V–T relaxation of excited HCN molecules in the presence of H_2O is studied and the consequences relevant to QEPAS-based HCN sensing are discussed.

2 Sensor configuration

QEPAS is based on the use of a quartz tuning fork (TF) as a sharply resonant and spatially selective microphone for detection of a photoacoustically generated sound. A general configuration of the QEPAS-based trace-gas sensor was described in [2]. Briefly, the target molecule in a gas sample is excited by the modulated laser light. Wavelength modulation at half the resonant frequency of the TF is performed. Commercially available TFs have a resonant frequency $f_{TF} \approx 32.8$ kHz, and therefore the laser wavelength modulation frequency must be set at $f_L = 1/2 f_{TF} \approx 16.4$ kHz. Lock-in detection of the TF-generated current at f_{TF} provides a value proportional to the concentration of the target species. This technique requires that the laser radiation is constantly in resonance with the molecular absorption, that is, locked to the target absorption line. Line locking is carried out by means of the reference cell with a high concentration of the target species and an optical detector. A $3f_L$ frequency component of the detector output serves as an error signal in the line-locking feedback loop. In the case of the semiconductor lasers which have been used in QEPAS experiments so far, the laser wavelength adjustment is performed simply by adjusting the laser injection current.

The configuration of the HCN sensor is shown in Fig. 1. A fiber-coupled distributed feedback diode laser (JDS Uniphase model CQF935/908-19600) was used as an excitation

✉ Fax: +1-713-348-5686, E-mail: akoster@rice.edu

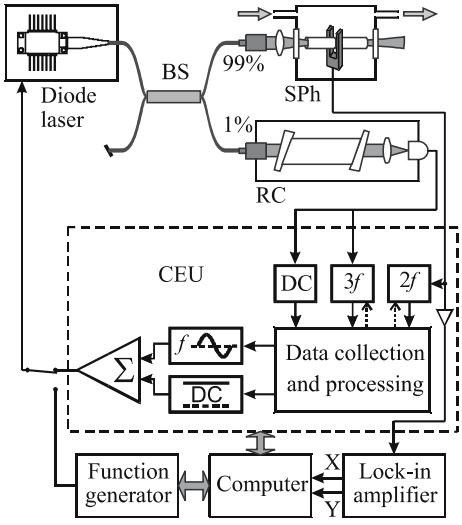

FIGURE 1 QEPAS-based HCN sensor. BS – fiber beam splitter, SPh – spectrophone in a vacuum-tight enclosure with optical windows and gas inlet and outlet, RC – reference cell with a built-in photodiode, CEU – control electronics unit

source. The HCN R6 transition of $2\nu_1$ at 6539.113 cm^{-1} was selected for monitoring purposes. The laser emission was split in a 1 : 99 ratio by means of a fiber beam splitter (ThorLabs 10202A-99-APC). A smaller fraction of the laser light was sent to a fiber-coupled reference cell assembly (Wavelength References, Mulino, Oregon) containing a sealed $l = 27$ mm cell filled with a mixture of 40 Torr HCN and 160 Torr N_2, a fiber collimator, and a lensed photodiode. The remaining laser power was directed to a spectrophone (called an 'absorption detection module (ADM)' in our earlier publication [2]) consisting of the TF and two pieces of glass tubing (inner diameter 0.4 mm) forming an acoustic microresonator. The spectrophone was placed into a vacuum-tight enclosure (the inner gas volume is $V \sim 1$ cm^3 when the spectrophone is installed) equipped with two sapphire windows and gas inlet and outlet. The optical power delivered to the spectrophone was measured to be 50 mW. The control electronics unit (CEU) performed the following functions:

- measuring f_{TF} and Q-factor of the TF;
- modulating the laser current (and hence its wavelength) at $f_L = 1/2 f_{TF}$;
- laser wavelength locking to the targeted absorption line;
- measuring the current generated by the TF in response to the photoacoustic signal.

The CEU has the capability to communicate with a computer via a RS232 serial data port. The normal operation mode of this sensor is when the laser is locked to the absorption line for continuous HCN concentration monitoring while the analyzed gas is flowing through the spectrophone chamber. This mode is feasible because of the background-free nature of QEPAS (see [2] and references therein). However, for sensor characterization purposes the data were sometimes acquired in the scan mode, when the dc component of the laser current and hence its wavelength were slowly scanned to acquire spectrally resolved data. To carry out such measurements, a computer-controlled function generator (SRS model DS345) was used to determine the diode laser current, and the TF response was detected using an auxiliary buffered TF output from the CEU and a lock-in amplifier.

A permeation tube based trace gas generator (Kin-Tek Laboratories, Inc., model 491M) was used for the sensor calibration. The generated HCN concentration in the carrier gas was determined by the gas mass flow rate through the device, reaching the maximum stable value of 6.25 ppmv at the minimum flow rate of 150 sccm. Of the total mass flow, 15–20 sccm of N_2:HCN was sampled into the spectrophone cell. Such a flow corresponds to a spectrophone cell flush approximately every 1.5 s at 300 Torr pressure and every 0.25 s at 60 Torr pressure in the cell. Thus, the sensor response time to changes in HCN concentration produced by the trace-gas generator was primarily determined by the adsorption–desorption processes in the connecting tubing, the valves, and the upstream pressure controller. The length of the $1/4''$ PTFE tubing was ~ 2 m, and the experimentally measured sensor response time was ~ 5 min (not counting the gas-propagation delay).

3 Experiments and results

Initially, a number of spectral scans near the R6 line of the $2\nu_1$ HCN overtone (CH stretch) [3] at 6539.11 cm^{-1} were performed at different pressures and laser current modulation indices while keeping the HCN concentration fixed at the 6.25-ppmv level, with the goal to determine conditions for the highest signal to noise ratio (SNR). It was found that the highest SNR is achieved at 300 Torr pressure when dry nitrogen was used as the HCN carrier gas, while using ambient (laboratory) air as a carrier resulted in a considerably higher SNR at 60 Torr. QEPAS data acquired at 60 Torr with air as a dilutant (50% relative humidity at +24 °C), 6.25-ppmv HCN, and optimum modulation index are presented in Fig. 2.

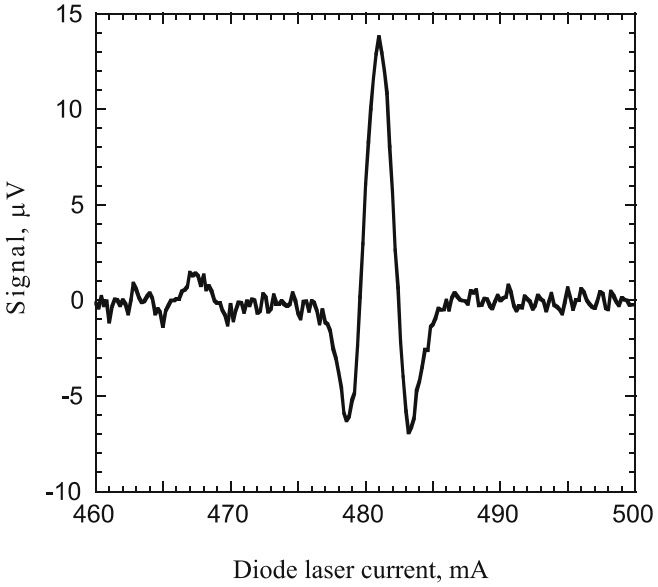

FIGURE 2 QEPAS data (transimpedance amplifier output voltage) recorded when the laser wavelength was scanned to encompass the HCN absorption line at 6539.11 cm^{-1} (the *larger line* in the center of the plot). The analyzed gas was ambient air doped with 6.25-ppmv HCN at a pressure of 60 Torr. A *weak line* to the left of the HCN line is an H_2O line at 6539.27 cm^{-1}

The lock-in amplifier (Stanford Research Systems model SR830 DSP) time constant was set to 1 s with a 18 dB/oct filter slope, which corresponds to an equivalent noise bandwidth of 0.19 Hz. The SNR calculated as a ratio of the peak signal to 1σ of the background noise is 40, which corresponds to a noise-equivalent concentration (NEC) of 155 ppbv. Based on the GEISA database and the online SPECTRA Information System (http://spectra.iao.ru, Institute of Atmospheric Optics, Russian Academy of Sciences), the normalized noise-equivalent absorption coefficient (NNEA) was calculated to be 4.3×10^{-9} cm^{-1} W/$\sqrt{\text{Hz}}$. Similarly, the calculated parameters when dry N_2 was used as the carrier gas at the optimum 300 Torr pressure are NEC = 330 ppbv and NNEA = 9.2×10^{-9} cm^{-1} W/$\sqrt{\text{Hz}}$. The same HCN detection sensitivity was calculated from the scatter of the CEU readings in a sequence of repeated measurements when the laser was locked to the peak of the absorption line.

A pronounced difference between the optimum conditions and the sensitivity for dry N_2 and ambient air is an indication that some components of air promote the V–T relaxation of HCN molecules. The most likely candidate is water vapor, which is known to increase the V–T relaxation rate of some molecules (see for example [4, 5]). Indeed, when synthetic dry air containing N_2, O_2, and CO_2 was used as the HCN carrier, the QEPAS signal amplitude, phase, and pressure dependence were the same as for pure N_2.

A setup shown in Fig. 3 was assembled to study the H_2O-induced relaxation in detail. Dry N_2 was bubbled through water with a controlled temperature set below room temperature of +24 °C. This moist N_2 flow was then mixed with the N_2:HCN flow from the trace-gas generator. The mixing ratio was controlled using two mass-flow meters. Finally, a 10-cm-long optical cell was installed after the spectrophone cell and the optical absorption of water at 7306.75 cm^{-1} was measured by means of a diode laser and a photodiode to verify the H_2O concentration in the gas.

The dependence of the QEPAS signal (amplitude and phase) on the H_2O concentration in the HCN carrying gas

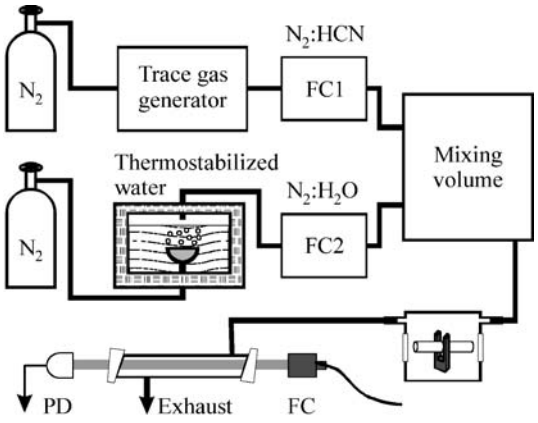

FIGURE 3 Setup for producing controlled concentrations of H_2O in a gas flow. FC1, FC2 – mass-flow controllers, FC – fiber collimator to couple the diode laser radiation at 1.37 μm into the optical gas cell, PD – photodiode

was measured at two pressures, 60 Torr and 300 Torr. The results are presented in Fig. 4. The measured QEPAS signal is normalized to the HCN concentration calculated from the dilution ratio. Fitting curves shown in Fig. 4 will be explained in Sect. 4.

4 Analysis of H_2O impact on QEPAS signal amplitude

We shall consider a simplified model of HCN V–T relaxation, assuming that it occurs as a one-stage process in collisions of HCN with either H_2O or N_2 molecules with the corresponding rate constants k_H and k_N:

$$\frac{\mathrm{d}[\mathrm{HCN}^*]}{\mathrm{d}t} = -k_H[\mathrm{HCN}^*][\mathrm{H_2O}] - k_N[\mathrm{HCN}^*][\mathrm{N_2}]\,, \qquad (1)$$

where [HCN*], [H_2O], and [N_2] are correspondingly the concentrations of the vibrationally excited HCN, H_2O, and N_2 molecules. We neglect collisions between two HCN molecules because of its low concentration. From this equa-

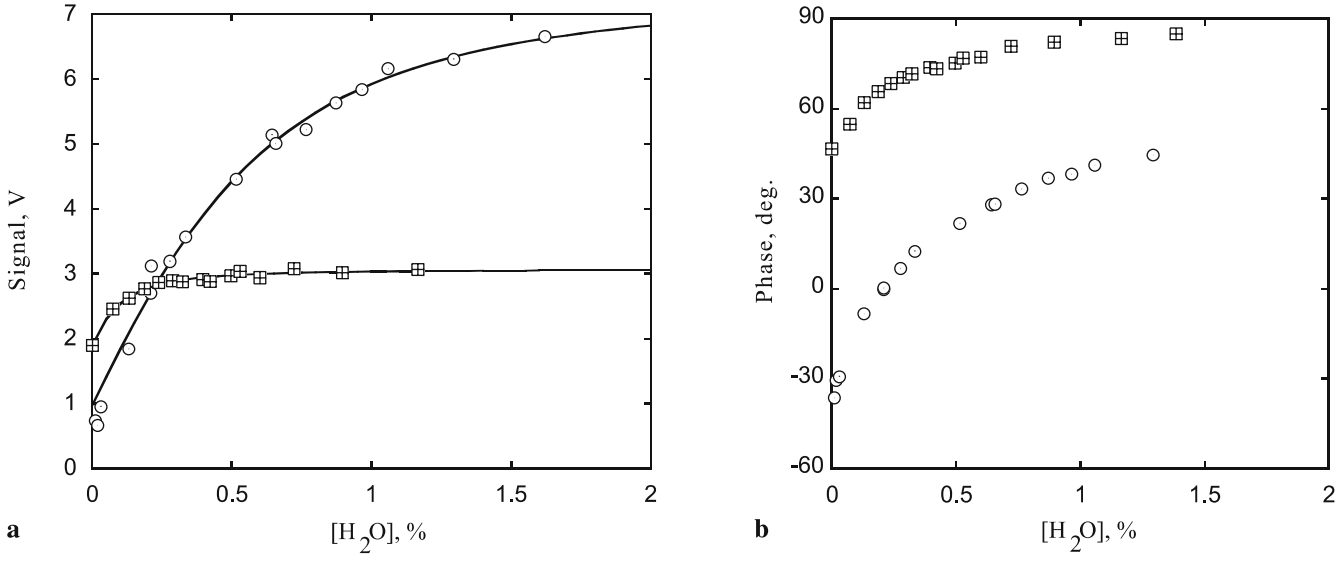

FIGURE 4 QEPAS signal amplitude (lock-in amplifier output voltage; **a**) and phase (**b**) upon diode laser excitation of HCN molecules as a function of the H_2O concentration in the carrier nitrogen. *Circles*: 60 Torr pressure, *squares*: 300 Torr pressure

tion, [HCN*] exhibits an exponential decay with a relaxation time

$$\tau = \frac{1}{k_{\mathrm{H}}[\mathrm{H_2O}] + k_{\mathrm{N}}[\mathrm{N_2}]} \,. \tag{2}$$

We can assume that $[N_2]$ does not depend on $[H_2O]$ because the fractional concentration x of $[H_2O]$ was always $x < 2\%$. Then, substituting x $[N_2]$ for $[H_2O]$ and $[N_2] = P/k_{\mathrm{B}}T$ molecules/cm^3 in (2) and defining $r = k_{\mathrm{H}}/k_{\mathrm{N}}$, we can rewrite (2) as

$$\tau = \frac{k_{\mathrm{B}}T}{Pk_{\mathrm{N}}} \frac{1}{1+rx} = \tau_0^{\mathrm{N}} \frac{P_0}{P} \frac{1}{1+rx} \,. \tag{3}$$

Here, $\tau_0^{\mathrm{N}} = k_{\mathrm{B}}T/P_0k_{\mathrm{N}}$ is the HCN* relaxation time in dry nitrogen at pressure P_0.

It is known [6, 7] that a photoacoustic signal S and its phase θ are related to the relaxation time as follows:

$$S = \frac{S_0}{\sqrt{1+(2\pi f\tau)^2}} \,, \tag{4}$$

$$\tan\theta = 2\pi f\tau \,, \tag{5}$$

where S_0 is the photoacoustic signal as it would be at an instantaneous relaxation ($\tau = 0$). The value of f denotes the modulation frequency of the optical excitation, which in our case is $f = f_{\mathrm{TF}} \approx 32.76$ kHz. Substituting the right-hand part of (3) for τ in (4), we obtain

$$S = \frac{S_0}{\sqrt{1+\left[\frac{A(P)}{1+rx}\right]^2}} \,, \tag{6}$$

$$A\,(P) = 2\pi f\tau_0^{\mathrm{N}} \frac{P_0}{P} \,. \tag{7}$$

The results of the experimental data fitted by the function (6) are presented in Table 1 along with the measured Q-factor of the TF, which determines the noise level. Data in the last row of Table 1 lists the normalized relaxation times of HCN in collisions with H_2O, which were obtained by regrouping the parameters in (6) so that $P_0\tau_0^{\mathrm{H}}$ is directly found as a fit parameter and not calculated from A and r in the same table, which would reduce the accuracy.

The HCN V–T relaxation parameters obtained from the experiments performed at two different pressures are consistent with each other, yielding a relaxation time of ~ 2 ms Torr in collisions with N_2 and ~ 1000 times more efficient relaxation in collisions with H_2O. The corresponding rate constant describing the thermalization of the initially populated second excited level of the C–H stretch vibration in HCN–N_2 collisions is $k_{\mathrm{N}} = 1.6\,\mathrm{cm}^3/(\mathrm{molecule\,s})$. Depopulation of this vibrational energy level of HCN was previously studied by Hastings et al. by means of time-resolved fluorescence [8]. They found this process rate constant to be $2.6 \pm 0.15\,\mathrm{cm}^3/(\mathrm{molecule\,s})$. This number is comparable to our measured k_{N} but expectedly higher, because complete thermalization includes not only $\nu_1 = 2$ level depopulation but also the subsequent V–T energy transfer from the lower-energy vibrational states.

It follows from these results that the QEPAS signal at 300 Torr will be above 90% of its maximum value when $[H_2O] > 0.18\%$ (6% relative humidity at +24 °C), while the same condition at 60 Torr is satisfied for $[H_2O] > 1.6\%$ (55% relative humidity at +24 °C).

Total pressure, Torr	60	300
Q_{TF}	18 200	11 000
S_0, V	7.31 ± 0.15	3.06 ± 0.02
r	930 ± 210	870 ± 100
A	7.4 ± 1.4	1.26 ± 0.05
$P_0\tau_0^{\mathrm{N}}$, ms Torr	2.2 ± 0.4	1.91 ± 0.07
$P_0\tau_0^{\mathrm{H}}$, µs Torr	2.3 ± 0.2	2.1 ± 0.2

TABLE 1 Measured Q-factor values and the model fit parameters for two gas pressures

5 Analysis of phase information

The photoacoustic signal is shifted in phase with respect to the optical excitation and, according to (5), this phase information can be used to study relaxation processes. In practice however the θ value is not measured directly but added to (or subtracted from) some angle φ, which we shall refer to as an instrument phase shift. In our case the measured phase was referenced to the antinode of the voltage sine wave applied to the laser driver modulation input; see Fig. 5. The following parts contributed to the instrument phase shift:

1. delay between the voltage change at the laser driver modulation input and the corresponding laser current change;
2. phase shift between the laser current and the laser wavelength;
3. 90° phase shift between the laser excitation and the photoacoustic response if $\tau = 0$ [6, 7];
4. phase shift added by the acoustic microresonator. If it does work like a harmonic oscillator (where pressure is considered as a coordinate), this shift must be 90° (see for example [9]);
5. uncertainty in the polarity of the TF, which can result in an additional 180° phase shift;
6. delay in the transimpedance amplifier, which is used to convert the TF current into voltage (not shown in Fig. 1).

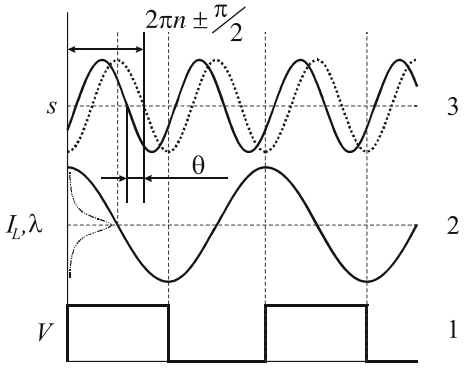

FIGURE 5 *Curves*: (1) synchronization signal for the lock-in reference (rising edge), (2) laser current and wavelength, with the absorption line envelope shown as a *dotted line* to the left, (3) photoacoustic signal: *dotted line* – in case of instant V–T relaxation, *solid line* – shifted because of the relaxation delay

Since the TF can be considered as an equivalent series resonant electrical circuit [2] and we detect the current in this circuit, the detected signal at resonant frequency is in phase with the applied force. If the shifts 1, 2, and 6 above are small (which is actually the case), relaxation is fast, and the acoustic resonator acts according to the idealized model, then the detected signal must be in phase with the energy input into the analyzed gas ($\varphi = 0$ or 180°). This case is illustrated in Fig. 5. The peak of the energy input into the gas coincides with the node of the modulated laser current. The lock-in amplifier used to measure the signal is configured so that the sine component is considered as the in-phase component, and therefore displays ±90° phase (+90° in our measurements) for a photoacoustic signal shown as solid curve 3 in Fig. 5, and $\pm 90^\circ - \theta$ if $\tau \neq 0$. Hence, the measured angle $\phi = 90^\circ - \tilde{\varphi} - \theta$, and

$$\theta = 90^\circ - \varphi - \phi \,. \tag{8}$$

The largest uncertainty in φ is associated with a phase shift in the acoustic microresonator. Its Q-factor and the related amplification can be small because of its small radius and the reduced gas pressure. The pressure acting on the TF is the sum of the pressure directly created by the immediate action of the laser excitation and the pressure oscillations in the microresonator. The second component is 90° ahead with respect to the first. Equation (5) can be rewritten as

$$g(P; x) = \frac{1}{\tan[90^\circ - \varphi(P) - \phi(x)]} = \frac{1}{A(P)}(1 + rx) \,. \tag{9}$$

Hence, if the experimentally measured values $\phi(x)$ are used in (9) with the correct pressure-dependent instrumental phase shift then $g(P; x)$ must be a simple linear function of the relative H_2O concentration x. We used this property of $g(P; x)$ to find the instrumental phase shift at two pressures, 60 Torr and 300 Torr. Parameters A and r were taken from Table 1, and φ was selected to result in the closest proximity of the experimental results to the linear function (9). As can be seen in Fig. 6, the phase data acquired at 300 Torr pressure are in good agreement with the developed relaxation model and indicate that the microresonator indeed provides a close to 90° phase shift ($\varphi \approx 0$). A similar procedure performed with the data acquired at 60 Torr pressure yielded $\varphi = 29^\circ$, and the phase measured at low H_2O concentration deviates from the linear relation (9). Deviations at lower [H_2O] probably result from model simplifications, namely a description of the multistage V–T relaxation process using only one kinetic equation with two rate constants.

The condition $\varphi \neq 0$ can be explained as a result of the above-mentioned superposition of the directly generated photoinduced pressure change P_{direct} and the microresonator oscillations P_{res}. These two components are orthogonal to each other, and hence $\tan(\varphi) = P_{\text{direct}}/P_{\text{res}}$. On the other hand, the microresonator Q-factor $Q_{\text{res}} = P_{\text{res}}/P_{\text{direct}}$. Thus, we have an estimate $Q_{\text{res}} = 1.8$. A theoretical evaluation of Q_{res} can be performed based on [10]. According to [10], the sound amplitude losses per unit length when sound is propagating through a pipe of radius r are

$$\alpha = \frac{\gamma'}{rc}\sqrt{\frac{\omega\eta}{2\rho}} \,, \tag{10}$$

where c is the speed of sound, $\omega = 2\pi f$, ρ is the gas density, η is the gas viscosity, and $\gamma' = 1 + (7/5)^{1/2} - (7/5)^{-1/2}$ for an ideal diatomic gas. Since the sound wave is propagating with a velocity c, the loss rate is αc and Q_{res} is

$$Q_{\text{res}} = \frac{r}{\gamma'}\sqrt{\frac{\pi\rho f}{\eta}} \,. \tag{11}$$

Substituting $\eta = 1.85 \times 10^{-5}$kg/(ms), $\rho = 0.093\,\text{kg/m}^3$ (both at +24 °C; ρ at 60 Torr), $r = 0.2$ mm, and $f = 32\,760$ Hz, we can calculate $Q_{\text{res}} = 3.4$. The experimentally evaluated $Q_{\text{res}} = 1.8$ is comparable to the calculated value but expectedly lower because the resonator used in our experiments is not a seamless half-wave pipe but has a gap in the center where the TF is placed.

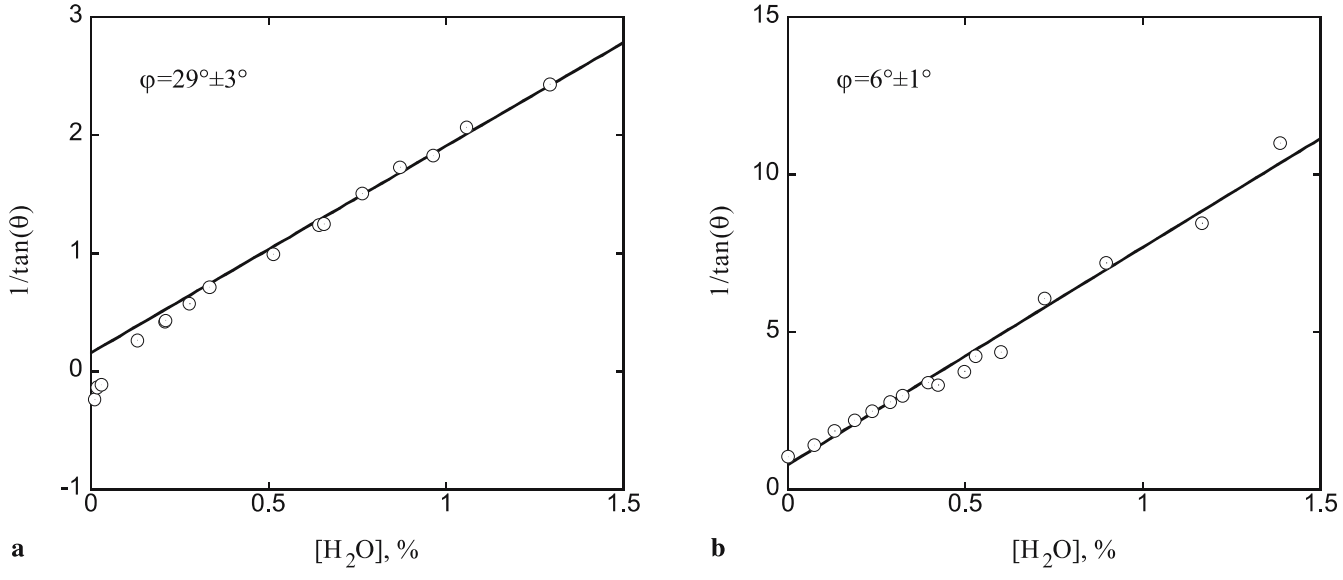

FIGURE 6 Observed phase of the photoacoustic signal approximated by the linear function $g(P; x)$: 60 Torr pressure (**a**) and 300 Torr pressure (**b**)

6 Conclusions

This investigation shows that the presence of moisture in the carrier gas significantly influences the QEPAS-based sensor response. However, if the data are acquired at 300 Torr pressure, the sensor response will remain within a 90%–100% range of its maximum in a wide span of [H_2O], from 6% relative humidity (+24 °C) and up. If a wider extent of conditions or a higher accuracy is required, the following approaches can be used:

1. measure humidity with an independent hygrometer and use a calibration table based on the present study;
2. dry the air sample before analysis. This will result in a reduced sensitivity to HCN compared to moist samples. If a molecular sieve filter is used for drying, there is a danger of HCN being trapped there, too. Using a Nafion-based dryer would require large amounts of drying gas;
3. humidify the sample before analysis. If the water content is close to 100% relative humidity at +24 °C, the sensitivity at 60 Torr determined by $S/\sqrt{Q_{TF}}$ will be 2.8 times higher than what can be achieved with dry samples (300 Torr).

The third approach seems to be the most attractive solution. A simple and compact humidifier can be realized based on Nafion tubes. With typical flow rates of 20 sccm used in this work a water supply of 100 g will suffice for more than 140 days of continuous operation.

The noise-equivalent concentration level of 155 ppbv with a 1-s time constant (or $\sim$ 3-s interval between uncorrelated readings) demonstrated in this work is significantly lower than the established exposure limit of 4.7 ppmv (see Sect. 1). If required, the sensitivity can be improved $\sim$ 2 times by installing a back-reflecting spherical mirror after the spectrophone gas cell to create a two-pass configuration, which was verified with a trace H_2O sensor of similar configuration (to be published). The detection threshold can also be lowered by increasing the sensor time constant, because the sensitivity-limiting noise scales inversely proportionally to the square root of the data-acquisition time [2]. In conclusion, QEPAS technology can be used for real-world HCN monitoring applications. A particular configuration of the sensor must be determined based on the environmental conditions and the requirements of its intended use.

ACKNOWLEDGEMENTS The authors acknowledge Dr. Bret Cannon of PNNL for his input into a theoretical estimate of the Q-factor of a pipe resonator. Financial support of the work performed by the Rice group was provided by DARPA via a subaward from Pacific Northwest National Laboratory (PNNL), Richfield, WA, the National Aeronautics and Space Administration (NASA), the Texas Advanced Technology Program, the Robert Welch Foundation, and the Office of Naval Research via a subaward from Texas A&M University.

REFERENCES

1 http://www.osha.gov/SLTC/healthguidelines/hydrogencyanide/recognition.html
2 A.A. Kosterev, F.K. Tittel, D. Serebryakov, A. Malinovsky, I. Morozov, Rev. Sci. Instrum. **76**, 043 105 (2005)
3 T. Shimanouchi, *Tables of Molecular Vibrational Frequencies*, consolidated Vol. I, Natl. Bur. Stand. (U.S.) National Standards References Data Series No. 39 (U.S. GPO, Washington, 1972)
4 F.G.C. Bijnen, F.J.M. Harren, J.H.P. Hackstein, J. Reuss, Appl. Opt. **35**, 5357 (1996)
5 S. Schilt, J.-P. Besson, L. Thévenaz, Appl. Phys. B **82**, 319 (2006)
6 G. Gorelik, Dokl. Akad. Nauk SSSR **54**, 779 (1946) [in Russian]
7 T.L. Cottrell, J.C. McCoubrey, *Molecular Energy Transfer in Gases* (Butterworths, London, 1961)
8 P.W. Hastings, M.K. Osborn, C.M. Sadowski, I.W. Smith, J. Chem. Phys. **78**, 3893 (1983)
9 T.L. Chow, *Classical Mechanics* (Wiley, New York Chichester Brisbane Toronto Singapore, 1995)
10 H.F. Olson, *Elements of Acoustical Engineering* (Van Nostrand, New York, 1947)